Analysis of a Corona-Discharge Based Electrostatic Motor

M. Abdel-Salam, A. Ahmed, H. Ziedan, and F. Diab
Electrical Engineering Department, Assiut University, Egypt

Abstract—This paper is aimed at proposing a new design of a corona-discharge based electrostatic motor with a cylindrical rotor made from aluminum foil and multi copper strip stator electrodes. The stator electrodes are alternately stressed positively and negatively. The onset voltage of corona discharge is calculated based on the condition of discharge sustenance at stator electrodes. The corona currents emitted from positively and negatively stressed electrodes are calculated being dependent on the applied voltage and motor geometry. This calls at first for calculation of the spatial distribution of electric field within the motor volume using the accurate charge simulation technique. The calculated corona onset voltage and current-voltage characteristics of the motor agreed reasonably with those measured experimentally for three motors built-in the laboratory. The dependency of the motor speed on the applied voltage is reported for the different investigated motors.

Keywords—Electrostatic motor, ionic wind, corona-discharge, field mapping, corona current, motor speed

I. Introduction

A. Previous Related Work

Historically speaking, the first electric motor invented was a corona-based electrostatic motor (ESM) and it was about 100 years before the conventional magnetic motor was conceived [1]. The ESM is characterized by simplicity of construction without winding and lightweight. The influence of corona electrodes' configurations on output torque was experimentally investigated in ESM with multi-blade electrodes [1]. The motor fabricated consisted of a 100 mm diameter hollow cylindrical rotor made of acrylic resin as a dielectric and several knife-blade corona electrodes with 100 mm length [1].

A micro ESM was fabricated [2] with sharp stator electrodes to ionize air molecules. The ions are transferred onto the rotor surface where coulomb repulsion between insulated rotor and electrodes result in a rotation of the rotor. Important design parameters, such as electrode spacing, air gap, and number of electrodes were studied [2] using an electrostatic field simulator. For good performance, the stator's electrodes should be axially thick with sharp tips [2]. Speed and torque were measured where the torque was estimated in the order of 10 nNm [2].

Corona motors are of interest in miniature applications because of their insensitivity to material properties and their ability to produce torque with DC excitation [3].

B. Aim of Paper

This paper is aimed at proposing an ESM with conducting cylindrical rotor and multi-stator electrodes and varying number of electrodes. The onset voltage of corona on stator electrodes and current-voltage characteristics are calculated and checked against those measured experimentally for built-in laboratory motor models. This calls at first for field calculation using the accurate charge simulation method. The dependency of the motor speed on the applied voltage is also investigated for the built-in motors.

Corresponding author: Mazen Abdel-Salam
e-mail address: mazen2000as@yahoo.com

II. The Proposed ESM

The proposed ESM has a cylindrical rotor of radius R made of aluminum foil, which rotates on the tip of a metal shaft having very small contact area so the friction loss is very small. The stator electrodes are strips capped with wedge at the tip, made from copper and insulated by cylindrical wooden shell of inner and outer radii R_1 and R_2, respectively, as shown in Fig. 1. The height of the wedge is h and that of the electrode is H. The gap spacing between the stator tip and the rotor surface is g. For two-dimensional analysis, the motor is assumed long enough when compared with the dimensions of the stator.

The principle of operation of the proposed ESM depends on the "Ionic Wind" phenomena [4-11]. Positive and negative high voltages stress the stator electrodes alternately. Subsequently, a strong electric field is

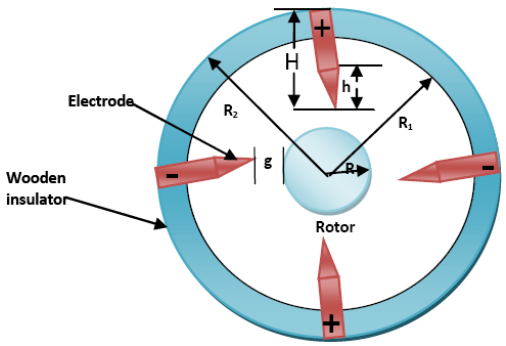

Fig. 1. Cross section of the proposed 4-electrode ESM.

generated near of the electrodes to form a corona discharge in air at electrode's tips. The air motion is created by the corona ions generated at the electrode, which drift either to the grounded rotor or to the nearby (surrounding) electrodes. Along their path, these ions collide with the electrically neutral air, transferring their momentum to air molecules resulting in the so-called "electric or ionic wind" [4-11]. Therefore, the ionic wind in this motor consists of two components:

The first component is the monopolar component, which is directed from the high voltage electrode toward the grounded rotor.

The second component is the bipolar one, which extends between the positive and negative electrodes.

These components are discussed for a motor with four-tilted electrodes. As regards the monopolar component, there is monopolar conduction of corona ions from each electrode to the grounded rotor associated with corona wind. The polarity of ions is the same as that of stressed electrode. The electrode tilting is aimed at producing bipolar component to the right side of the electrode different from that of the left side. This will help in generating a torque to run the rotor as explained in the following paragraphs.

As regards the bipolar component, there is conduction of positive ions from each positive electrode to the bounding (surrounding) negative electrodes associated with ionic wind from the positive to the negative electrodes in the direction F_{ab}, F_{ad}, F_{cb}, and F_{cd}. In addition, there is conduction of negative ions from each negative electrode to the surrounding positive electrodes associated with ionic wind in the directions F_{ba}, F_{bc}, F_{da}, and F_{dc}. The flow of ionic wind in the directions F_{ab}, F_{ad}, F_{cb}, and F_{cd} are opposite to that in the direction F_{ba}, F_{bc}, F_{da}, and F_{dc} as shown in Fig. 2.

The ionic wind associated with positive ions flow is greater than that due to negative ions' flow [10-13]. This is attributed to the lower mobility assigned to positive ions when compared with that of negative ions [14].

The smaller the mobility of ions, the more is the residence time of the ions drifting between the positive and negative electrodes, and the more the time available for the ions to transfer their momentum to the air molecules with subsequent increase of the flow of ionic wind. This ends up with a net flow of ionic wind in the directions F_{ab}', F_{ad}', F_{cb}', and F_{cd}' as shown in Fig. 3.

Because of electrode tilting to the left, the electric field to the left of the electrode and the associated ionic wind is higher than those of the right of the electrode. Therefore, the ionic wind in the direction F_{ab}' is larger than F_{ad}'. In other words, the ionic wind from electrode (a) dominates in the direction F_{ab}'' toward electrode (b) as shown in Fig. 4. Similarly, the ionic wind from electrode (c) dominates in the direction F_{cd}'' toward electrode (d).

The ionic wind in the direction F_{ab}'' and F_{cd}'' as shown in Fig. 4 has a gradient along the radial direction toward the axis of the rotor resulting in a shear force [15-18] tangent to the rotor. Such shear force drives the rotor to run in the direction a b c d, i.e. clockwise direction.

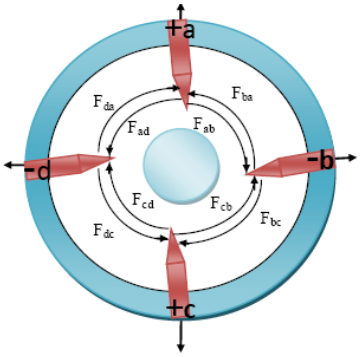

Fig. 2. Bipolar forces in 4-electrode motor due to ionic wind.

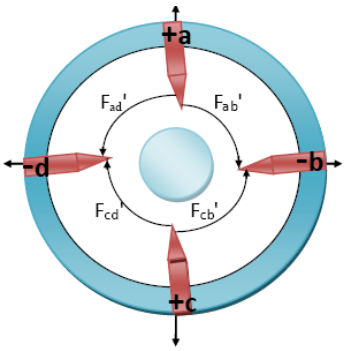

Fig. 3. Resultant positive and negative bipolar forces in 4-electrode motor due to ionic wind.

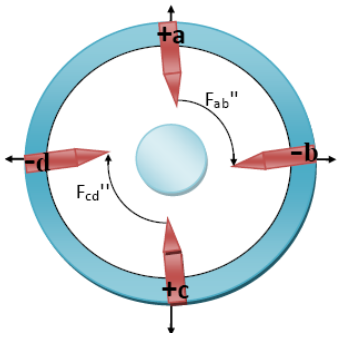

Fig. 4. Dominating bipolar forces in 4-electrode motor due to ionic wind.

III. Corona Onset Voltage Calculation in ESM

It has been demonstrated that the onset voltage of negative corona in rod-to-plane and point-to-plane gaps is smaller than that of positive corona [14, 19, 20]. Therefore, negative corona takes place first in the proposed ESM. With the increase of the voltage applied on the stator electrodes, the electric field near electrodes' tips reaches the threshold value for ionization of gas molecules by electron collision [21]. An electron avalanche starts to develop along the direction of maximum field, which extends toward the rotor as shown in Fig. 5. With the growth of the avalanche, more electrons are developed at its head, more photons are emitted in all directions, and more positive ions are left in the avalanche wake. For a successor avalanche to be started, the preceding avalanche should somehow

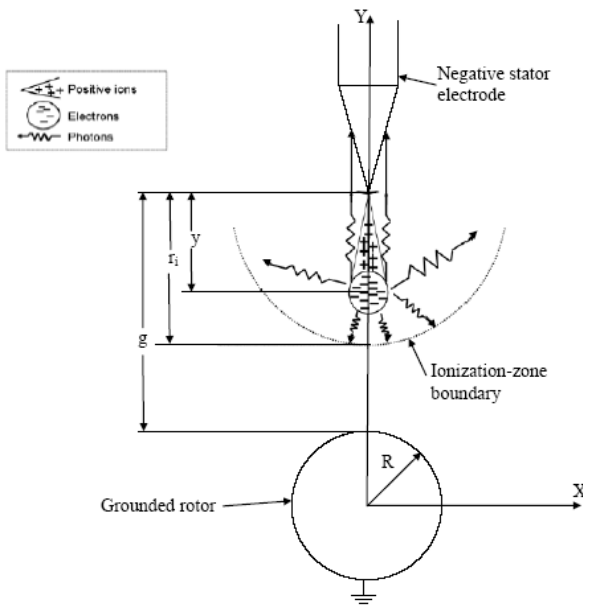

Fig. 5. Development of avalanche at one of ESM electrodes.

provide an initiating electron at the cathode surface, possibly by photoemission, positive ion impact, metastable action, or field emission. Field emission is possible only at field strengths exceeding 5×10^7 V/m [22]. Electron emission by positive ion impact is more than two orders of magnitude less probable than photoemission [23]. Metastables have been reported to have an effect approximately equal to that of positive ion impact [24, 25]. Therefore, only the first mechanism (electron emission from the cathode by photons) was considered in the mathematical formulation of the onset criterion, where at least one photoelectron is emitted by the photons of the first avalanche to keep the discharge self-sustained, i.e.,

$$N_{\text{eph}} \geq 1 \tag{1}$$

where N_{eph} is the number of electrons photo-emitted from the cathode.

The onset voltage does not appear explicitly in the relation (1) and the onset voltage is the critical value which fulfills the Eq. (1) [22].

The condition for a new (successor) avalanche to develop [26, 27] is:

$$\gamma_{\text{Ph}} \left(\int_{R+g}^{R+g-r_i} \alpha(y) \exp[D] G(y) \exp[-\mu y] \, \mathrm{d}y \right) \geq 1 \tag{2}$$

where

$$D = \int_{R+g}^{R+g-y} (\alpha - \eta) \, \mathrm{d}y$$

R is the motor rotor radius as shown in Fig. 5.
g is the gap spacing between the stator tip and the rotor surface as shown in Fig. 5.
r_i is radius of the ionization zone boundary as shown in Fig. 5.
y is the axial distance travelled by the avalanche starting at the tip of the stator electrode as shown in Fig. 5.
G is a geometry factor to account for the fraction of photons received by the stator electrode.
α is the Townsend's first ionization coefficient (Appendix A, [28]).
γ_{Ph} is the coefficient of electron emission by the action of photons (Appendix A, [28]).
μ is the coefficient of photon absorption (Appendix A, [28]).
η is the electron attachment coefficient (Appendix A, [28]).

IV. Method of Analysis

The corona currents are calculated for applied voltages V above the onset value V_o.

Due to the alternative polarity of the electrodes, there are two components of corona current:

1. Monopolar component.
2. Bipolar component.

A. Calculation of Monopolar Corona Current Component

The monopolar component of corona current is convected between each stator electrode and the grounded rotor.

A.1. Describing Equations

Based on Deutsch's assumption [29], the electric field E in the presence of space charge and the space-charge-free field E' are related as

$$E = \mathcal{L}E' \tag{3}$$

where $\mathcal{L}$ is a scalar point function of the space coordinates depending on charge distribution.

The equations describing the electric field and the ionic flow are

$$\nabla E = \rho/\varepsilon_0 \tag{4}$$
$$J = k\rho E \tag{5}$$
$$\nabla J = 0 \tag{6}$$

where
ρ is the volume space-charge density (C/m^3).
ε_0 is permittivity of free space (=(1/36π)×10^{-9} (F/m)).
k is the mobility of ions (= 1.5×10^{-4} (m^2/V.s)).
J is the current density (A/m^2)

The first is Poisson's equation for the electric field, the second is the equation for current density, and the third is the equation of current continuity. Thermal diffusion of ions is neglected.

A.2. Boundary Conditions

A.2.1. Boundary Conditions at the Electrodes

Voltage without space charge $\varphi = \pm V$.
Voltage with space charge $\Phi = \pm V$.
The ratio E/E' is $\mathcal{L}_e$ ($=V_o/V$).

A.2.2. Boundary Conditions at Rotor Surface

Voltage without space charge $\varphi = 0$.
Voltage with space charge $\Phi = 0$.

Mathematical manipulation of Eqs. (3) through (6) results in the following expressions which determine distribution of the ion charge density ρ and the scalar $\mathcal{L}$ along the field lines emanating from stator electrodes to the grounded rotor.

$$1/\rho^2 = (1/{\rho_e}^2) + (2/\varepsilon_0\rho_e\mathcal{L}_e)\int_{\phi}^{V} \mathrm{d}\phi/(E')^2 \quad (7)$$

$$\mathcal{L}^2 = {\mathcal{L}_e}^2 + (2\rho_e\mathcal{L}_e/\varepsilon_0)\int_{\phi}^{V} \mathrm{d}\phi/(E')^2 \quad (8)$$

where ρ_e is the volume space-charge density at the electrode surface (C/m^3).

Eqs. (7) and (8) are to be integrated along the electric field lines which extend from the corona electrodes to the grounded rotor. An iterative procedure was proposed before [29] to determine the charge density ρ_e at the corona electrode surface.

After convergence, one can calculate the monopolar current density where a field line emanates from the stator electrode surface to the grounded rotor as:

$$J_{\text{monopolar}} = k\rho_e E_{\text{smono}} \quad (9)$$

where E_{smono} is the electric field at electrode surface, where monopolar corona takes place.

The mobility value of ions is chosen depending on the polarity of the electrode.

The monopolar corona current conducted through a flux tube, whose axis is the field line, is obtained as:

$$I_{\text{monopolar tube}\pm} = J_{\text{monopolar tube}\pm}\Delta s \quad (10)$$

where Δs is the longitudinal normal surface area of the flux tube.

The monopolar corona current per positive or negative electrode is obtained as:

$$I_{\text{monopolar elec.}\pm} = \sum I_{\text{monopolar tube}\pm} \quad (11)$$

where the summation takes place over all flux tubes along them the monopolar corona ions convect around the surface of stator electrode.

The motor monopolar corona current is obtained by summing the current emitted from all electrodes as:

$$I_{monopolar\ motor} = \sum \text{No. of pairs elec.} \left(I_{monopolar\ elec.+} + I_{monopolar\ elec.-}\right) \quad (12)$$

where the number of positively-stressed electrodes is equal to that of the negatively-stressed electrodes.

B. Calculation of Bipolar Corona Current Component

The bipolar component of corona current is convected between neighboring electrodes. To calculate the bipolar component of current, the idealized model proposed before [14] is adopted. In the idealized model, symmetry around the zero potential plane between two successive electrodes is considered. The zero potential plane is considered as one of the boundaries in solving the equations of the ionized field. The boundary value problem therefore be solved only between $\varphi = 0$ and $\varphi = V$ instead of between $\varphi = -V$ and $\varphi = V$ at both positive and negative electrodes.

B.1. Describing Equations

These equations are based on assuming equal mobility of both positive and negative ions and equal corona onset voltage at both the positive and negative electrodes ($V_{o+} = V_{o-} = V_o$).

$$\mathrm{d}\Phi/\mathrm{d}\varphi = \mathcal{L} \quad (13)$$

$$\mathrm{d}\rho_+/\mathrm{d}\varphi = \rho_+(\rho_+ - C_1\rho_-)/\varepsilon_0\mathcal{L}E'^2 \quad (14)$$

$$\mathrm{d}\rho_-/\mathrm{d}\varphi = -\rho_-(\rho_- - C_1\rho_-)/\varepsilon_0\mathcal{L}E'^2 \quad (15)$$

$$\mathrm{d}\mathcal{L}/\mathrm{d}\varphi = -(\rho_+ - \rho_-)/\varepsilon_0 E'^2 \quad (16)$$

$$C_1 = 1 - (\varepsilon_0 R_i/ke) \quad (17)$$

where

ρ_+ the volume space-charge density of positive ions (C/m^3)
ρ_- the volume space-charge density of negative ions (C/m^3)
R_i the recombination coefficient of the ions, $R_i = 2.2 \times 10^{-12}$ (m^3/s)
e the electron charge, $e = 1.6\times10^{-19}$ (C)
K_+ the mobility of positive ions (m^2/V.s)
K_- the mobility of negative ions (m^2/V.s)
V_{o+} the positive corona onset voltage (V)
V_{o-} the negative corona onset voltage (V)
$K_+ = K_- = K = 1.5\times10^{-4}$ (m^2/V.s)

B.2 Boundary conditions

The boundary conditions at the electrodes and rotor surfaces are the same as those for the monopolar corona current component.

Summitry in the idealized model dictates that the volume charge density at the zero potential is expressed to the surrounding electrodes as:

$$\rho_+ = \rho_- = \rho_o \quad (18)$$

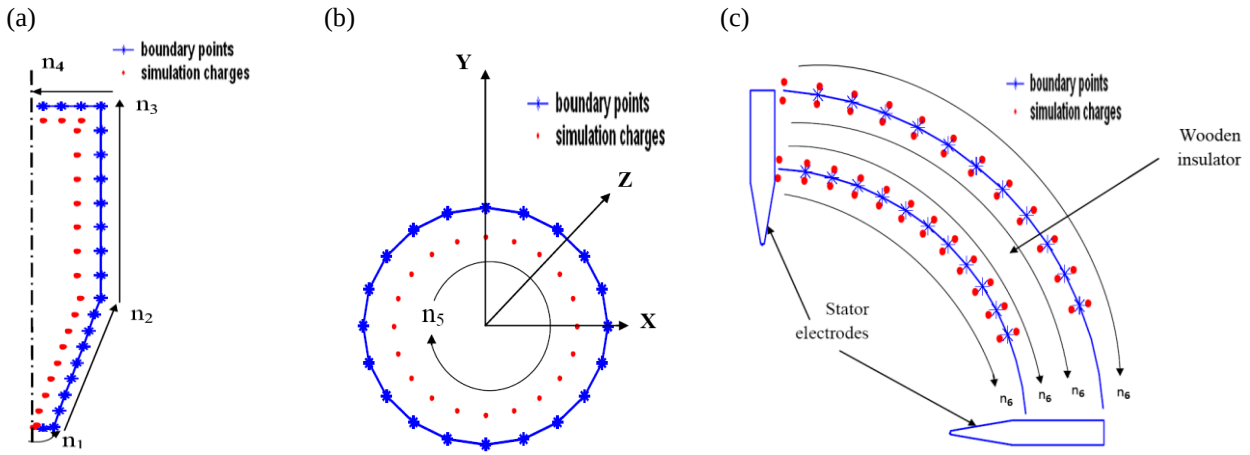

Fig. 6. (a) Cross-section of one electrode showing simulation charges and associated boundary points. (b) Cross-section of the rotor showing simulation charges and associated boundary points.(c) Cross-section of the wooden insulator between two stator electrodes showing simulation charges and associated boundary points.

Integrating Eqs. (13) through (17) along the electric field lines starting from zero potential plane (midway between the positive and negative electrodes) determines the distribution of the ion charge density ρ and the scalar $\mathcal{L}$ using the iterative procedure proposed before [14].

After convergence, one can calculate the bipolar current density where a field line emanates from the stator electrode surface as:

$$J_{bipolar} = k_{+}\rho_{+}E_{sbi} + k_{-}\rho_{-}E_{sbi} \qquad (19)$$

where E_{sbi} is the electric field at the electrode surface, where bipolar corona takes place.

The bipolar corona current conducted through a flux tube whose axis is the field line, is obtained as:

$$I_{bipolar\ tube\ \pm} = J_{bipolar\ \pm}\Delta s \qquad (20)$$

The bipolar corona current per electrode is obtained as:

$$I_{bipolar\ elec.\pm} = \sum I_{bipolar\ tube\ \pm} \qquad (21)$$

where the summation takes place over all flux tubes, along them the bipolar corona ions convect around the surface of stator electrode.

The motor bipolar corona current is obtained as:

$$I_{bipolar\ motor} = \sum No.of\ elec.\left(I_{bipolar\ elec.\pm}\right) \qquad (22)$$

The motor total corona current is obtained as:

$$I_{motor} = \sum\left(I_{monopolar\ motor} + I_{bipolar\ motor}\right) \qquad (23)$$

V. ELECTIRC FIELD CALCULATION

Integrating the describing equations for monopolar and bipolar coronas along the field lines is requested to determine the current-voltage characteristics of the ESM. Therefore, the field around the stator electrodes is mapped. Some field lines emanating from the electrode terminate at the grounded rotor. Along these field lines, the corona ions convect from the stressed electrode to the grounded rotor forming the monopolar component of the corona current. Other field lines emanating from the electrode terminate at the neighboring electrodes with opposite polarity. Along these field lines, positive and negative ions convect forming the bipolar component of the corona current.

The charge simulation technique [30-32] is used to map the electric field lines, which emanate from the stressed electrodes. As the ESM is assumed infinitely long in the Z axial-direction, infinite line charges extending parallel to the motor axis were used to simulate the conducting stator electrodes and cylindrical rotor. Each electrode is symmetrical about its axial midway plane, so the surface charges on each side of the electrode are the same. The surface charge on each side of the stator electrode is simulated by n_1 line charges for the electrode tip, n_2 line charges for the wedge side, n_3 line charges for the strip side and n_4 line charges for the electrode base, Fig. 6(a). These charges are positioned inside the electrode. Thus, the number of simulation charges per electrode is $2(n_1 + n_2 + n_3 + n_4)$ as shown in Fig. 6(a). The surface charge on the rotor is simulated by a number n_5 line charges distributed uniformly inside the rotor as shown in Fig. 6(b). The surface charge on the wooden insulating material between two successive electrodes is simulated by four sets of line charges each of n_6 line charges. Two sets are positioned inside the dielectric and the other two sets in air as shown in Fig. 6(c). To evaluate the simulation charges, boundary points are selected on the surface of the stator electrodes and the rotor, where a boundary point is assigned to a simulation charge of the stator electrodes and rotor. Other boundary points are chosen on the wooden insulator surface, where a boundary point is assigned to two simulation charges. The location of line charges takes place according to assignment factor $F_a = a_2/a_1$ [31],

where a_1 is the distance between two successive boundary points and a_2 is the distance between the boundary point and the corresponding simulation charge. Therefore, the total number N of unknowns simulation charges is: $2n_e(n_1 + n_2 + n_3 + n_4) + n_5 + 4n_e n_6$ where n_e is the number of stator electrodes.

The boundary conditions are: (i) The calculated potential at the boundary points selected on the stator electrodes is equal to the applied voltage. (ii) The calculated potential at the boundary points selected on the rotor surface is equal to zero. (iii) The calculated potential at the boundary points selected on the insulator surface is the same whether seen from the air or insulator sides. (iv) The continuity of the electric flux at the boundary points selected on the insulator surface is satisfied. Satisfaction of the boundary conditions at the electrodes, rotor and insulator surfaces results in a set of simultaneous equations whose solution determine the unknown simulation charges. Once the simulation charges are known, one can evaluate the spatial distribution of the electric field and trace the field lines emanating from the stressed electrodes.

VI. Experimental Setup

The proposed ESM has a cross-sectional view as shown in Fig. 1. The setup to test the proposed ESM was built-in the high voltage laboratory of Assiut University. Dimensions of the proposed ESM models are given in Table I, where the sum of the rotor radius R and the gap spacing g is constant (= 0.06 m).

The set-up consists of:

(1) Auto transformer with input 220 V AC, and variable output voltage from 0 to 220 V.
(2) HV transformer steps the voltage up to the desired value in the range from 0-100 kV.
(3) Half-wave positive and negative high-voltage rectifier circuit composed of two 20 mA, 140 kV PIV diodes and 10 nF, 140 kV smoothing capacitor. The DC voltage is applied across a 280 MΩ resistance in series with a micro-ammeter for measuring the generated DC voltage. Positive and negative voltages are applied alternately to the ESM electrodes through 0.5 MΩ water resistance to limit the current in case of a flashover occurs.

The corona current was measured using sensitive micro-ammeter connected to the stressed electrodes.

A Faraday cage was built-in to accommodate the micro-ammeter, thus shielding it to ensure no corona discharge on its hardware as shown in Fig. 7(a).

VII. Results and Discussions

A. Corona Onset-Voltages

Table II shows how the corona onset voltage of the proposed ESM changes with rotor radius for different number of stator electrodes. The corona onset voltage decreases with the increase of rotor radius as the gap spacing between the tip of stator electrode and rotor surface decreases irrespective of the number of stator electrodes. This reflects itself on increase of the electric field and decrease of the corona onset voltage. The table shows a good agreement of the measured corona onset voltage with those calculated according to the condition of discharge sustenance at stator electrodes as expressed by Eq. (2).

TABLE I
DIMENSIONS OF THE PROPOSED ESM

ESM #	R_1 (m)	R_2 (m)	g (m)	h (m)	H (m)
1	0.09	0.11	0.02	0.04	0.05
2	0.09	0.11	0.025	0.035	0.05
3	0.09	0.11	0.035	0.025	0.05

TABLE II
CORONA ONSET-VOLTAGE OF THE PROPOSED THREE ESMS

ESM #	#1: N=2 electrodes		#2: N=4 electrodes		#3: N=8 electrodes	
Radius of rotor R (m)	V_{om}- (kV)	V_{calc}- (kV)	V_{om}- (kV)	V_{calc}- (kV)	V_{om}- (kV)	V_{calc}- (kV)
0.02	11.2	12	8.4	9.2	4.8	5.2
0.025	10	10.5	7.6	8.3	4.4	4.7
0.035	8	8.8	5.6	6.1	3.5	3.78

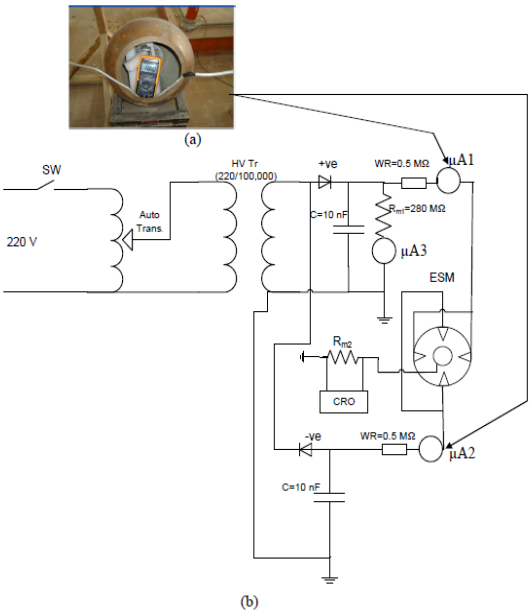

Fig. 7. (a) Faraday cage to shield the digital micro-ammeter, (b) Schematic diagram of experimental model of ESM.

B. Current-Voltage Characteristics

B.1. Corona current as influenced by number of stator electrodes

It is quite clear that the calculated and measured corona currents increase with the increase of number of stator electrodes irrespective of the gap spacing between the stator electrodes and rotor surface, as shown in Figs.

8-10. This is attributed to the increase of the electric field at the tip of stator electrodes with the increase of the number of stator electrodes with a subsequent increase of the corona current at the same value of applied voltage.

B.2. Corona current as influenced by the gap spacing

The calculated and measured corona currents increase with the decrease of the gap spacing between the stator electrodes and rotor surface irrespective of the number of stator electrodes, as shown in Figs. 11-13. This is attributed to the increase of the electric field at the tip of stator electrodes with the decrease of the gap spacing with a subsequent increase of the corona current at the same value of applied voltage. Figs. 8-13 show a good agreement of the measured current-voltage characteristics with those calculated.

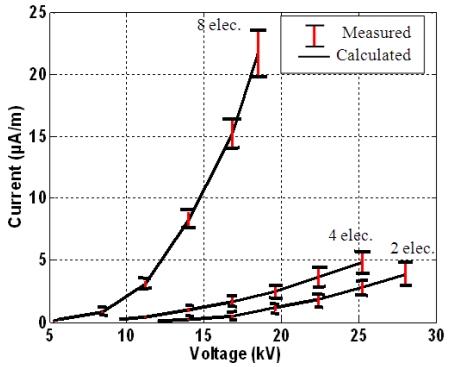

Fig. 8. Measured and calculated corona current of different number of stator electrodes (g = 0.04(m) and R = 0.02(m)) ESM.

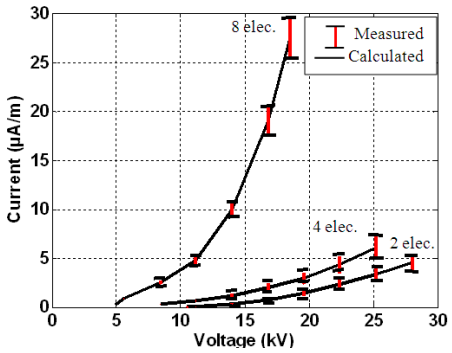

Fig. 9. Measured and calculated corona current of different number of stator electrodes (g = 0.035(m) and R = 0.025(m)) ESM.

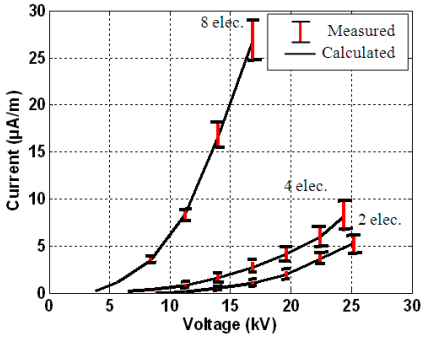

Fig. 10. Measured and calculated corona current of different number of stator electrodes (g = 0.025(m) and R = 0.035(m)) ESM.

C. Speed-Voltage Characteristic

Figs. 14-19 show how the speed of the proposed ESM changes with the applied voltage at different gaps spacing and different numbers of electrodes provided that the sum of gap spacing and rotor radius is constant (R+g = 0.06 (m)). The scatter of the measured speed values did not exceed 5%. The speed increases with the increase of the voltage at the same gap spacing. This is attributed to the increase of the corona current and the associated ionic wind with the increase of the applied voltage. With the decrease of the gap spacing, the corona

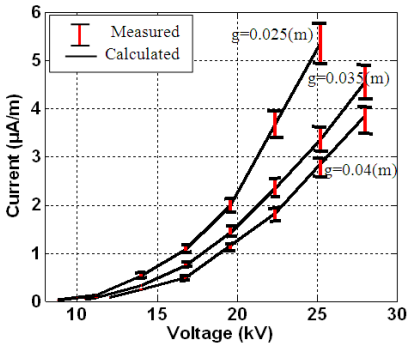

Fig. 11. Measured and calculated corona current of different gaps spacing (N=2-electrodes) ESM.

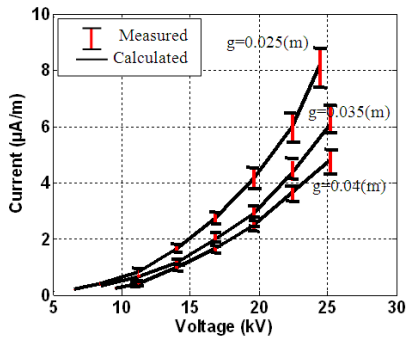

Fig. 12. Measured and calculated corona current of different gaps spacing (N=4-electrodes) ESM.

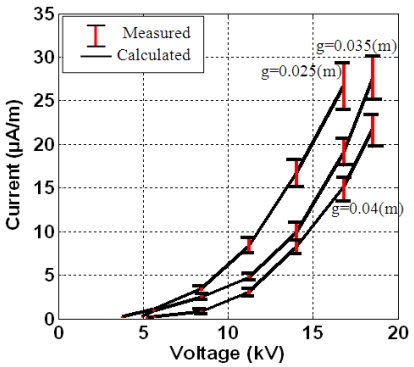

Fig. 13. Measured and calculated corona current of different gaps spacing (N=8-electrodes) ESM.

current and associated wind increase at the same applied voltage with a subsequent increase of the ESM speed.

The voltage V_s at which the motor starts to rotate decreases with the decrease of the gap spacing irrespective of the number of electrodes. V_s decreases with the increase of the number of electrodes for different gaps spacing. This is attributed to the increase of the corona current and the associated ionic wind, so the motor can start rotation at smaller voltage.

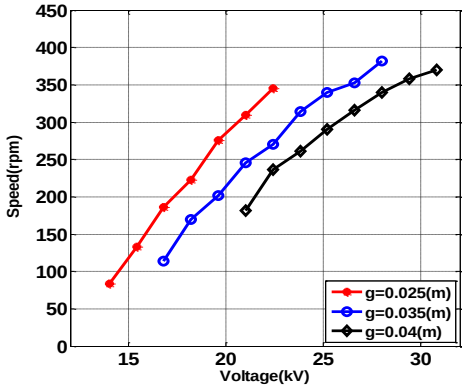

Fig. 14. Speed-voltage characteristics for 2-electrode ESM with different gaps spacing.

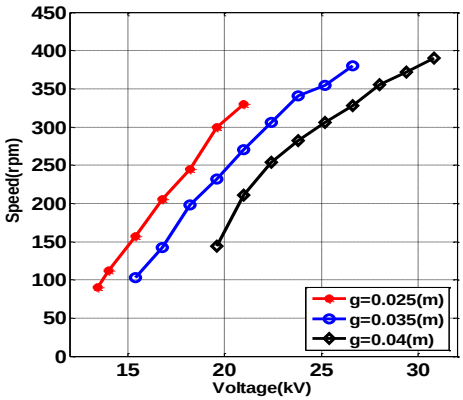

Fig. 15. Speed-voltage characteristics for 4-electrode ESM with different gaps spacing.

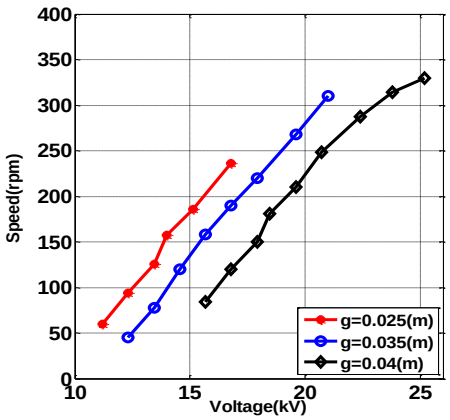

Fig. 16. Speed-voltage characteristics for 8-electrode ESM with different gaps spacing.

VIII. Conclusions

Based on the analysis presented in this paper, the following conclusions may be drawn:

1) A new design of a corona-discharge based electrostatic motor with a cylindrical rotor made

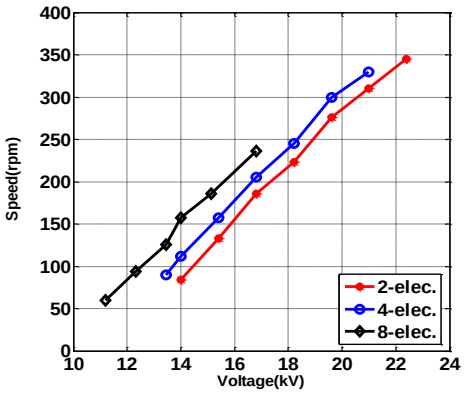

Fig. 17. Speed-voltage for 2, 4, and 8 electrode ESM (R = 0.035 (m), g = 0.025 (m)).

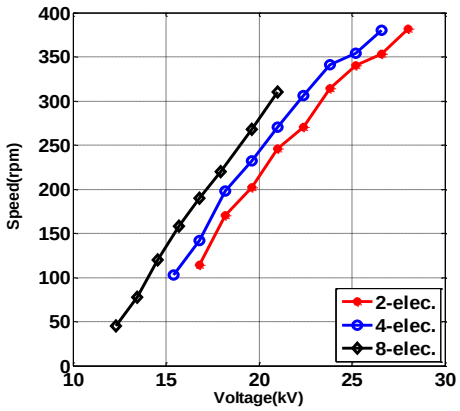

Fig. 18. Speed-voltage for 2, 4, and 8 electrode ESM (R = 0.025 (m), g = 0.035 (m)).

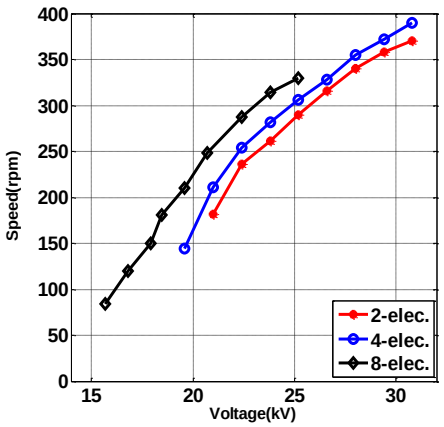

Fig. 19. Speed-voltage for 2, 4, and 8 electrode ESM (R = 0.02 (m), g = 0.04 (m)).

from aluminum foil and multi strip stator electrodes from copper is proposed. The stator electrodes are 2, 4 and 8 in number and alternately stressed positively and negatively.

2) The spatial distribution of electric field for field mapping within the motor volume is determined using the accurate charge simulation technique.
3) The onset voltage of negative corona discharge is calculated based on the condition of discharge sustenance at stator electrodes.
4) The corona currents emitted from the positively and negatively stressed electrodes are calculated being dependent on the applied voltage and motor geometry.
5) The calculated corona onset voltage and current-voltage characteristic of the motor agreed reasonably with those measured experimentally for three motors built-in the laboratory.
6) The motor speed increases with the increase of the applied voltage for the investigated three motors.

APPENDICES

Appendix A. Discharge Parameters

In order to calculate the onset voltage of corona on each stator electrode at atmospheric pressure, the relation (2) was solved using the values available in the literature [28], for α, η, γ_{Ph} and μ. The equations relating α (cm^{-1}) and η (cm^{-1}) at pressure P (torr) to the electric field E (V/cm) were expressed as:

$$\eta = P\left(0.01298 - \left(0.541 \times 10^{-3}(E/P)\right) + \left(0.87 \times 10^{-5}(E/P)^2\right)\right) \quad \text{(A.1)}$$

$$\alpha = 4.778P\, e^{-221(P/E)} \quad \text{if } 25 \le E/P \le 60 \quad \text{(A.2)}$$

$$\alpha = 9.682P\, e^{-264.2(P/E)} \quad \text{if } 60 \le E/P \le 240 \quad \text{(A.3)}$$

The coefficient of photon absorption μ was taken 5 (cm^{-1}) [28]. The coefficient of electron emission by photons γ_{Ph} was taken 3×10^{-3} [28].

REFERENCES

[1] M. Hattori, K. Asano, and Y. Higashiyama, "The fundamental characteristics of a cylindrical corona motor with multi-blade electrodes," *Journal of Electrostatics*, vol. 27, pp. 223-235, 1992.

[2] S. Lee, D. Kim, M. D. Bryant, and F. F. Ling, "A micro corona motor," *Sensors and Actuators A-Physical*, vol. 118, pp. 226-232, 2005.

[3] P. T. Krein, "Analysis of Corona Motors and Micromotors by Means of Effective Gap Conductivity," *IEEE Transactions on Industry Applications*, vol. 31, pp. 752-760, 1995.

[4] M. Rickard, D. Dunn-Rankin, F. Weinberg, and F. Carleton, "Characterization of ionic wind velocity," *Journal of Electrostatics*, vol. 63, pp. 711-716, 2005.

[5] A. B. Vatazhin, V. A. Likhter, and K. E. Ulybyshev, ""Ion wind", a gas-dynamic flow in the corona discharge, and its interaction with the external flow," *Fluid Dynamics*, vol. 47, pp. 206-213, 2012.

[6] O. D. Jefimenko, *Electrostatic Motors*, Electret Scientific Company, Morgantown, West Virginia, 1973, pp. 56-72.

[7] J. Mizeraczyk, M. Kocik, J. Dekowski, M. Dors, J. Podliński, T. Ohkubo, S. Kanazawa, and T. Kawasaki, "Measurements of the velocity field of the flue gas flow in an electrostatic precipitator model using PIV method," *Journal of Electrostatics*, vol. 51–52, pp. 272-277, 2001.

[8] A. A. Martins, "Modeling of an EHD corona flow in nitrogen gas using an asymmetric capacitor for propulsion," *Journal of Electrostatics*, vol. 69, pp. 133-138, 2011.

[9] N. Sakakibara, T. Hattori, K. Miura, H. Noguchi, A. Fukami, and T. Nabeta, "Air cleaner using ionic wind," U.S. Patent 4643745, 1987.

[10] A. A. Martins, "Modelling of an improved positive corona thruster and actuator," *Journal of Electrostatics*, vol. 71, pp. 61-67, 2013.

[11] H. Kalman and E. Sher, "Enhancement of heat transfer by means of a corona wind created by a wire electrode and confined wings assembly," *Applied Thermal Engineering*, vol. 21, pp. 265-282, 2001.

[12] R. Ianconescu, D. Sohar, and M. Mudrik, "An analysis of the Brown-Biefeld effect," *Journal of Electrostatics*, vol. 69, pp. 512-521, 2011.

[13] A. A. Martins and M. J. Pinheiro, "On the nature of the propulsive force of asymmetric capacitors in the atmosphere," *Physics Procedia*, vol. 20, pp. 103-111, 2011.

[14] M. P. Sarma and W. Janischewskyj, "Analysis of Corona Losses on DC Transmission Lines Part II - Bipolar Lines," *IEEE Transactions on Power Apparatus and Systems*, vol. PAS-88, pp. 1476-1491, 1969.

[15] B. R. Muson, D. F. Young, T. H. Okihi, and W. W. Huebch, *Fundamentals of Fluid Mechanics*, Wiley, New York, Chichester, Brisbane,Toronto, Singaphore, 2006, pp. 1-31.

[16] S. K. Som and G. Biswas, *Introduction to Fluid Mechanics and Fluid machines*, Tata Mc Graw-Hill Publishing Company limited, New Delhi, India, 2003, pp. 1-27.

[17] R. W. Fox and A. T. Mcdonald, *Introduction to Fluid Mechanics*, Wiley, New York, Chichester, Brisbane, Toronto, Singapore, 1985, pp. 1-35.

[18] A. J. Chorin and J. E. Marsden, *A Mathematical Introduction to Fluid Mechanics*, Springer, Limited, London, UK, 2012, pp. 47-95.

[19] R. J. Van Brunt and M. Misakian, "Mechanisms for Inception of DC and 60-Hz AC Corona in SF6," *IEEE Transactions on Electrical Insulation*, vol. EI-17, pp. 106-120, 1982.

[20] W. N. English, "Positive and Negative Point-to-Plane Corona in Air," *Physical Review*, vol. 74, pp. 170-178, 1948.

[21] M. Abdel-Salam, H. Anis, A. E. Morshedy, and R. Radwan, *High Voltage Engineering Theory and Practice*, Marcel Dekker, Inc., New York, USA, 2000, pp. 149-184.

[22] M. Khalifa, M. Abdel-Salam and Abou-Seade, "Calculation of negative corona onset voltage," *IEEE PES conference paper*, vol. C-73, pp.160-169, 1973.

[23] L. B. Loeb, *Electrical Coronas: Their Basic Physical Mechanisms*, University of California Press, Berkeley, CA, USA, 1956, pp. 299-359.

[24] E. Nasser, *Fundamentals of Gaseous Ionization and Plasma Electronics*, Wiley-Inter science, New York, USA, 1971, pp. 24-101.

[25] M. Abdel-Salam, H. Anis, A. E. Morshedy, and R. Radwan, *High Voltage Engineering Theory and Practice*, Marcel Dekker, Inc., New York, USA, 2000, pp. 81-112.

[26] M. Abdel-Salam and E. K. Stanek, "On the calculation of breakdown voltages for uniform electric fields in compressed air and SF_6," *IEEE Transactions on Industry Applications*, vol. 24, pp. 1025-1030, 1988.

[27] M. Abdel-Salam and D. Wiitanen, "Calculation of corona onset voltage for duct-type precipitators," *IEEE Transactions on Industry Applications*, vol. 29, pp. 274-280, 1993.

[28] M. P. Sarma and W. Janischewskyj, "D.C. corona on smooth conductors in air. Steady-state analysis of the ionisation layer," *Proceedings of the Institution of Electrical Engineers*, vol. 116, pp. 161-166, 1969.

[29] M. P. Sarma and W. Janischewskyj, "Analysis of Corona Losses on DC Transmission Lines: I - Unipolar Lines," *IEEE Transactions on Power Apparatus and Systems*, vol. PAS-88, pp. 718-731, 1969.

[30] M. Abdel-Salam, H. Anis, A. E. Morshedy, and R. Radwan, *High Voltage Engineering Theory and Practice*, Marcel Dekker, Inc., New York, USA, 2000, pp. 9-80.

[31] H. Singer, H. Steinbigler, and P. Weiss, "A Charge Simulation Method for the Calculation of High Voltage Fields," *IEEE Transactions on Power Apparatus and Systems*, vol. PAS-93, pp. 1660-1668, 1974.

[32] H. Ziedan, A. Sayed, A. Mizuno, and A. Ahmed, "Onset voltage of corona discharge in wire-duct electrostatic precipitators," *International Journal of Plasma Environmental Science & Technology*, vol. 4, pp. 36-44, 2010.